Jurnal Asiimetrik: Jurnal Ilmiah Rekayasa Dan Inovasi
Terakreditasi "**Peringkat 3"** berdasarkan SK Dirjendiktiristek, Nomor: 225/E/KPT/2022
Volume 5 Nomor 2 Tahun 2023, Juli 2023, Halaman 251-262
Website : http://journal.univpancasila.ac.id/index.php/asiimetrik/

p-ISSN 2655-1861
e-ISSN 2716-2923

Analisis Penggunaan *Bio Flap* pada NACA 4415 dengan Metode Numerik

Analysis of the Use of Bio Flap on NACA 4415 with Numerical Methods

James Julian[1*], Saphira Anggraita Siswanto[1], Fitri Wahyuni[1] dan Nely Toding Bunga[2]
[1]Mechanical Engineering, Universitas Pembangunan Nasional Veteran Jakarta, Jawa Barat 12450, Indonesia
[2]Program Studi Teknik Mesin, Fakultas Teknik, Universitas Pancasila, Jakarta 12640, Indonesia

Article information:

Received:
06/03/2023
Revised:
03/04/2023
Accepted:
18/04/2023

Abstract

This study was conducted using the Computational Fluid Dynamics (CFD) method using the Reynolds Averaged Navier Stokes (RANS) approach. The type of airfoil used in this study is the asymmetry NACA 4415 airfoil type. In this paper, computational tests were carried out on the airfoil with the addition of bionic flaps on its trailing edge. This study's update tests three variations of the Reynolds number: Re = 10^6, Re = 5 × 10^5, and Re = 3 × 10^5. The airfoil test was carried out at AoA 0°-25°. The addition of bionic flaps causes a decrease in lift performance at low AoA, but at high AoA, it can increase lift performance on airfoils. In addition, adding a bionic flap on the airfoil can delay the occurrence of a stall. At AoA 10°-13°, the Cd of the three variations of the Reynolds number experiences an increase in performance. Then, from this computational test, the resulting Coefficient moment (Cm) is a pitch down because the torque is below zero.

Keywords*: aerodynamics, airfoil, bionic flaps, NACA 4415, Reynolds number.*

***SDGs*:**

9 INDUSTRY, INNOVATION AND INFRASTRUCTURE

Abstrak

Studi ini dilakukan dengan menggunakan metode Computational Fluid Dynamics (CFD) dengan menggunakan pendekatan Reynolds Averaged Navier Stokes (RANS). Tipe airfoil yang digunakan pada studi ini adalah jenis airfoil asymmetry NACA 4415. Pada paper ini, uji komputasional dijalankan pada airfoil dengan tambahan bionic flaps pada trailing edge nya.keterbaruan dari penelitian ini adalah dengan pengujian menggunakan 3 variasi bilangan Reynolds Re = 10^6 , Re = 5 × 10^5, dan Re = 3 × 10^5. Uji airfoil dilakukan pada AoA 0°-25°. Penambahan bionic flaps menyebabkan penurunan performa lift pada AoA rendah, namun pada AoA tinggi dapat meningkatkan perform lift pada airfoil. Selain itu, penambahan bionic flap pada airfoil dapat menunda terjadinya stall. Pada AoA 10°-13° drag dari ketiga variasi bilangan Reynolds mengalami peningkatan performa. Kemudian, dari uji komputasional ini, momen yang dihasilkan mengalami pitch down karena torsi berada dibawah nol.

Kata Kunci: *aerodynamics, airfoil, bionic flaps*, NACA 4415, Reynolds number.

*Correspondence Author
email : zames@upnvj.ac.id

1. INTRODUCTION

An airfoil is a geometric shape of the cross-section of an airplane wing (He *et al.*, 2019; Li, Bouhlel and Martins, 2019; Supriya *et al.*, 2019; Zhang *et al.*, 2015). On airplanes, many phenomena occur. The condition when the plane takes off has a lot of big influences that play a role in the process (Bardera-Mora *et al.*, 2019; Zhao and Sushama, 2020). Like the aerodynamics formula, an airplane requires lower pressure on the upper side and higher pressure on the lower side to fly. In this phenomenon, when the plane takes off, it needs a large Coefficient lift (Cl) to be lifted (Kumar and German, 2022; Müller *et al.*, 2014; Radespiel and Heinze, 2014). For this reason, many trials have been carried out to improve the performance of Cl on airfoils. Testing the airfoil by modifying the trailing edge using a flap is often done to find out the aerodynamic effect it produces (Julian *et al.*, 2022; Nair and Goza, 2022; Wu *et al.*, 2022).

Studies that discuss the matter of airfoils are so interesting to discuss. With various modifications, it can have a different impact on the airfoil. One of the most exciting airfoil modifications to discuss is a modification inspired by nature. Xinyu et al. once discussed an adaptation of the NACA 0012 airfoil by using an owl-like flap named OWL05, stating that an owl-like airfoil can increase Cl during an airfoil downstroke (Lang *et al.*, 2021). Altman and Guillaume conducted an artificial flap with Re = 2 × 10^5 using an airfoil that formed bird feathers on a NACA 0012 airfoil to test the increase in post-stall performance (Altman and Allemand, 2016). The result was an increase in post-stall Cl performance at an angle of 5% to 30% (Altman and Allemand, 2016). Xie et al. examined Gurney flaps at Re = 10^4 by varying their height (Xie *et al.*, 2016). They stated that increasing the height causes a higher Coefficient drag (Cd) (Xie *et al.*, 2016). Another study by Nair and Goza on deployable flaps noted that the Cl increased by as much as 30% compared to the baseline observed when the flaps were in the mid-chord (Nair and Goza, 2020).

The above study has the same topic as this paper, discussing airfoils with modified flaps. The flap modification in this paper is inspired by the features of a bird's wings. To optimize the Cl of the airfoil, it is necessary to test its lift and drag force. Therefore, this paper tries to examine the airfoil by adding a flap on the back of an airfoil. In this study, the airfoil used is the NACA 4415 type. The NACA 4415 airfoil is a type of airfoil that is classified as four digits. The 4-digit airfoil is most frequently used in wind turbines, aircraft wings, and other airfoil applications (Rubel *et al.*, 2016; Julian *et al.*, 2023). NACA 4415 is an airfoil that is widely applied to various aerodynamic devices. This phenomenon is due to the stability and ability of NACA 4415 b to reduce drag at high speeds (Raymer, 2018). However, this airfoil is unsatisfactory at low Reynolds numbers such as Re = 10^6, Re = 5 × 10^5, dan Re = 3 × 10^5. So, this study tries to improve the ability of NACA 4415 at low speeds. Thus, the utilization of NACA 4415 becomes wide. Using computational methods, this study uses variations of the Reynolds number Re = 10^6, Re = 5 × 10^5, dan Re = 3 × 10^5. The interpretation of the Reynolds number on the airfoil is tested from various Angles of Attack (AoA) angles. In this study, the sample AoA used is an angle of 0° to a rise of 25°. Therefore, this study aimed to determine the effect of flaps on variations in the Reynolds number with an AoA angle of 0° - 25°. The reason for taking AoA samples up to a slope of 25° is because this slope is an extreme angle of attack for aircraft during take-off conditions. Flow control devices are used to improve airfoil performance at low Reynolds numbers. The flow control devices itself is divided into two types, namely active flow control and passive flow control. So far, studies have investigated active flow control devices such as co-flow jets, suction controls, and blow controls (James *et al.*, 2018; Zhang *et al.*, 2017; Zhao *et al.*, 2015) . From existing research, active control devices are proven to be effective in improving airfoil aerodynamics. However, active flow control devices require actuating devices to run. This is what reduces the efficiency of using active flow control. As an alternative, passive flow control devices can be used as they do not require actuating devices. One example of using a passive flow control device is the bionic flap. Studies on the use of bionic flaps have been carried out several times by varying the shape of the flaps. So far, no studies have investigated variations in Reynolds number in modified bionic flaps. Therefore, this study attempts to fill this void.

2. METHODOLOGY

This paper uses the Computational Fluid Dynamics (CFD) method. This study conducted a study on the NACA 4415 airfoil. The outline of this research is shown in Figure 1. Meanwhile, three main steps are carried out, namely pre-processing, processing, and post-processing in pre-processing, starting with making the NACA 4415 airfoil geometry and its modifications using bionic flaps. After that, the geometry is continued for the meshing process. After the meshing has been successfully executed, set the boundary conditions around the geometry; then, all data is taken in the processing process and will be tested through a grid independence test. If the grid independence test results fail, all steps must be repeated from the meshing because there may be errors in the meshing process and the processes after it (Iskandar and Julian, 2022). If the grid independence test results are successful, then the next step is to analyze and draw conclusions. The conclusions drawn will be the result of this study.

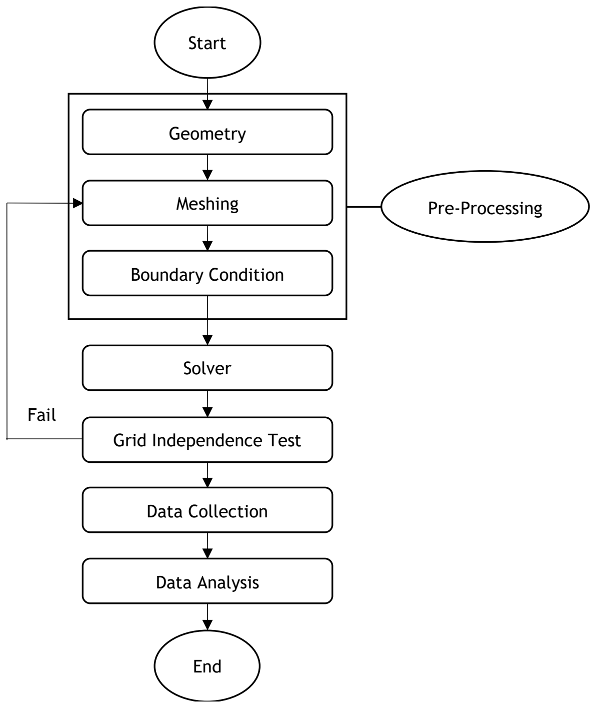

Figure 1. Flowchart

2.1. NACA 4415 Airfoil Modification

NACA 4415 airfoil is an asymmetrical airfoil shape. Different geometry of the NACA 4415 airfoil can be seen in Figure 2. The length of the chord airfoil used is 1 m. In this study, the rear part of the airfoil chord was modified using CAD software by adding a bionic flap inspired by the features of a bird's wing.

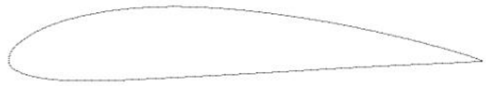

(a). Airfoil without bionic flap

(b). Airfoil with bionic flap

Figure 2. Model simulation

2.2. Governing Equation

The Reynold Averaged Navier Stokes (RANS) approach is used to solve the mathematical equations in this study. The RANS equation depends on many things, one of which is the turbulence model (Xiao *et al.*, 2016). The turbulence model used in this study is k-ε. K in this turbulence model is used to calculate the turbulent kinetic energy, while ε is used to calculate the dissipation rate of the turbulence velocity. The mathematical equation of RANS can be seen in equations 1 and 2 (Aftab *et al.*, 2016), while the mathematical equation of the k-ε turbulence model is shown in equations 3 and 4 (Lew†, Buscaglia and Carrica, 2001).

$$\frac{\partial \rho}{\partial t} + \frac{\partial}{\partial x_i}(\rho u_i) = 0 \tag{1}$$

$$\frac{\partial}{\partial t}(\rho u_i) + \frac{\partial}{\partial x_i}(\rho u_i u_j) = \frac{\partial p}{\partial x_i} + \frac{\partial}{\partial x_j}\left[\mu\left(\frac{\partial u_i}{\partial x_j} + \frac{\partial u_j}{\partial x_i} - \frac{2}{3}\delta_{ij}\frac{\partial u_i}{\partial x_j}\right)\right] + \frac{\partial}{\partial x_i}\left(\rho \overline{u'_i u'_j}\right) \tag{2}$$

$$\frac{D}{Dt}(\rho k) = \frac{\partial}{\partial x_j}\left[\left(\mu + \frac{\mu_t}{\sigma_k}\right)\frac{\partial k}{\partial x_j}\right] + G_k - \rho\varepsilon \tag{3}$$

$$\frac{D}{Dt}(\rho \varepsilon) = \frac{\partial}{\partial x_j}\left[\left(\mu + \frac{\mu_t}{\sigma_\varepsilon}\right)\frac{\partial \varepsilon}{\partial x_j}\right] + C_{el}\frac{\varepsilon}{k}G_k - \rho C_{\varepsilon 2}\frac{\varepsilon^2}{k} \tag{4}$$

2.3. Coefficient Lift and Coefficient Drag

One thing that is never separated when discussing the aerodynamics of an airfoil is its lift and drag. An airfoil will not work if there is no aerodynamic force affecting it. The C_l has a vector whose direction is perpendicular to the direction of the freestream flow (Julian *et al.*, 2022). It is this C_l that causes the airfoil to have the ability to fly. The C_d has a vector in the same direction as the freestream velocity (Julian *et al.*, 2016; Karim and Julian, 2018). Mathematical calculations for C_d and C_l are shown by equations 5 and 6 (Alom, Borah and Saha, 2018).

$$C_D = \frac{F_D}{\frac{1}{2}\rho A(V-u)^2} \quad (5)$$

$$C_L = \frac{F_L}{\frac{1}{2}\rho A(V-u)^2} \quad (6)$$

Where F_d = Force of Drag; F_l = Force of Lift; ρ = Mass of density; V = Flow velocity of the object; and A = Cross-sectional area of the object.

2.4. Domain and Boundary Condition

In this study, the domains used are rectangles and semicircles. The boundary conditions around the airfoil and bionic flaps are stationary (no slip) walls. The boundary condition around the domain is called velocity inlet. At the same time, the outlet is called the pressure outlet. The outlet pressure used in this study is zero, while the inlet velocity adjusts to the Reynolds number used. Figure 3 shows the NACA 4415 airfoil with 1 m chord and boundary conditions used in this study.

2.5. Mesh Independence Test

The mesh used in this study is a quadrilateral mesh type. This type of mesh is used because it has advantages in terms of computational efficiency. In addition, this type of mesh is easier to make in a structured mesh form than the quadrilateral mesh type. There are three types of mesh variations used in this study. Fine mesh with 200,000 elements, medium mesh with 100,000 elements, and coarse with 50,000 elements. These three types of mesh will be tested in the mesh independence test stage to select the most appropriate kind of mesh. These three types of mesh are visualized in Figure 4.

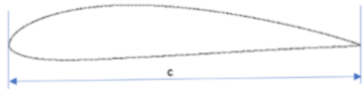

(a). Airfoil NACA 4415

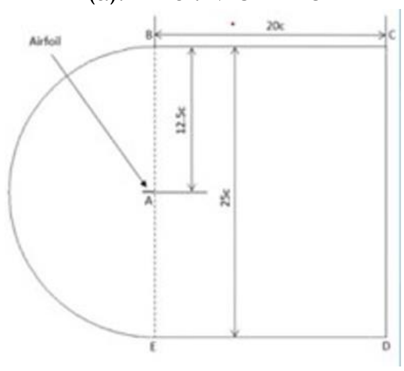

(b). Boundary condition

Figure 3. Model domain and boundary condition

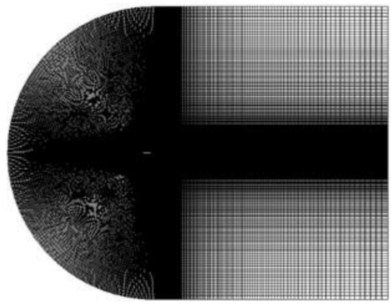

(a). Fine

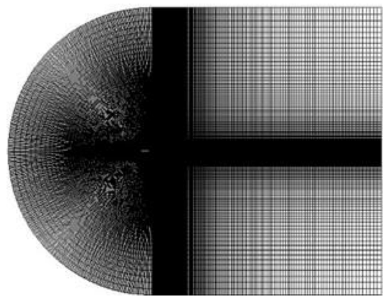

(b). Medium

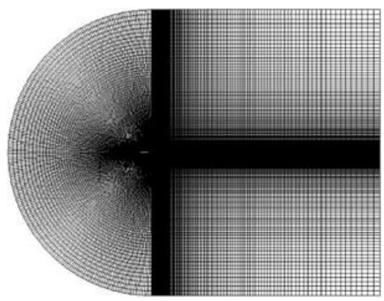

(c). Coarse

Figure 4. Variations of mesh

This study used a method generalized by Roache, namely the Richardson extrapolation method, to perform the mesh independence test. The initial stage in this test is to find the ratio of the grid variations used (Roache, 1994). The calculation can be found in equation 7. After that, determine the order using equation 8. After the order is obtained, the stages can be continued by determining the Grid Convergence Index (GCI) to find errors in a grid. In this paper, there are 2 GCIs used. GCI_{fine} is used to calculate the error between the fine and medium mesh, as shown in equation 9.

Meanwhile, GCI_{coarse} is used to calculate errors arising between the medium and coarse mesh, as shown in equation 10. The grid independence test must comply with two aspects. The first aspect is to analyze whether the variation of the mesh used is within the concurrent range. This range can find this using equation 11. Then the second aspect is to determine which mesh is the best. The mesh with the smallest error value for the parameter is the best mesh category, which will be used in this study, shown by equation 12 (Roache, 1994).

$$r = \frac{h_2}{h_1} \tag{7}$$

$$\bar{\bar{p}} = \frac{ln\left(\frac{f_3-f_2}{f_2-f_1}\right)}{ln(r)} \tag{8}$$

$$GCI_{fine} = \frac{F_S|\epsilon|}{(r^{\bar{\bar{p}}}-1)} \tag{9}$$

$$GCI_{coarse} = \frac{F_S|\epsilon|r^{\bar{\bar{p}}}}{(r^{\bar{\bar{p}}}-1)} \tag{10}$$

$$\frac{GCI_{coarse}}{GCI_{fine}r^{\bar{\bar{p}}}} \approx 1 \tag{11}$$

$$f\,r_{h=0} = f_1 + \frac{((f_1-f_2\,))}{(r^{\bar{\bar{p}}}\,-1)} \tag{12}$$

Data collection for the mesh independence test was carried out at coordinates X = 0.5 and Y = 0.15. The results of the mesh independence test are shown in Table 1. It can be seen that $\frac{GCI_{coarse}r^{p}}{GCI_{fine}} \approx 1$ so that the mesh variation can be said convergent. Furthermore, the mesh that has the lowest error is the fine mesh which is 0.0322%.

Table 1. Grid independency study result

Mesh	Fine	Medium	Coarse
Velocity	17.5593	17.5475	17.5111
$\bar{\bar{p}}$		1.625151591	
R		2	
GCI_{fine}		0.040%	
GCI_{coarse}		0.1244%	
$f_{rh} = 0$		17.56496	
$\frac{GCI_{coarse}}{GCI_{fine}r^{\bar{\bar{p}}}}$		1.00000	
Error	0.0322%	0.0994%	0.3066%

3. RESULTS AND DISCUSSION

To validate the accuracy of this study, a comparison of computational data with experimental data by Hoffman (Hoffmann, Reuss Ramsay and Gregorek, 1996) was used. Comparisons were made on the NACA 4415 computational baseline airfoil data. A comparison of the C_l from the computational and experimental data is shown in Figure 5a. the comparison indicates that the increase in C_l from the two pieces of information is not much different. Still, a significant difference begins to occur at an AoA angle of 10°, which is more difficult to detect. In predictions, the stalls of both data occur at angles AoA which are not much different, but the computational data stalls 1° faster than the experimental data. Then, the C_d of both computational and experimental data is shown in Figure 5b. In Figure 5b, it can be seen that there is no significant difference between the two data. Both move up as AoA increases. From the results of C_d and C_l, it can be concluded that the results are satisfactory, so the computational data used is valid.

This study uses data management and comparison methods from several variations of the Reynolds number. The geometry model used in this study is the NACA 4415 airfoil with a modified bionic flap. This study uses three variations of the Reynolds number in the process: Re = 10^6, Re = 5 × 10^5, dan Re = 3 × 10^5. The data analyzed from this study include data on the C_d, C_l, and C_m. The AoA studied range from 0°-25°.

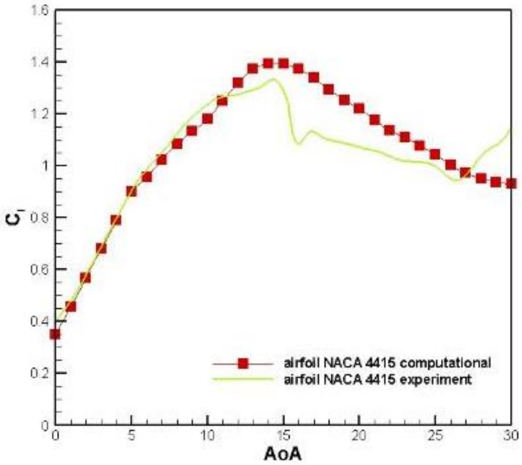

(a). Graph of C_l against changes AoA

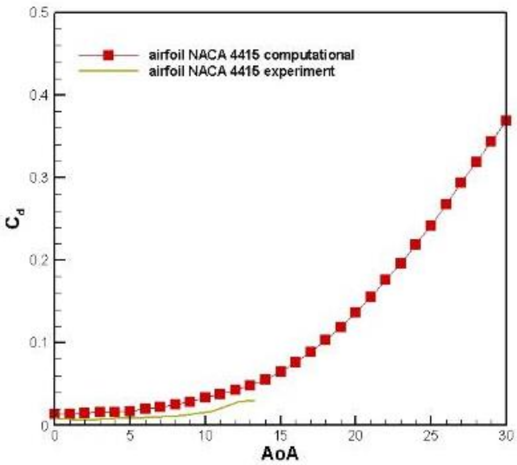

(b). Graph of C_d against changes AoA

Figure 5. Validation C_l and C_d

Data from the C_d and C_l tests are shown in Figure 6. It can be seen from the C_l curve the processing data generated from the NACA 4415 baseline, and the bionic flap modification are not much different. The baseline with Reynolds numbers Re = 10^6 , Re = 5 × 10^5, dan Re = 3 × 10^5 indicates a stall at AoA = 15°. In the modified bionic flap with Reynolds numbers Re = 5 × 10^5 and Re = 3 × 10^5, there is congestion at 1° slower than the baseline. In the bionic flap with Reynolds number Re = 10^6, the maximum C_l is achieved at AoA = 16°, which is the highest point compared to the other 5 data. The resulting C_l tends to be lower than the baseline in the bionic flap modification, but the stall from the baseline occurs faster than in the bionic flap modification.

In the C_d curve, the same thing happens with the C_l curve. There are no significant changes from the six airfoil data presented. The C_d of the six constant data rises with a difference that is not much difference between the airfoils. However, the data of the three airfoils with the bionic flap modification show a higher C_d than the baseline C_d so the drag efficiency of the baseline is slightly better than the bionic flap modification.

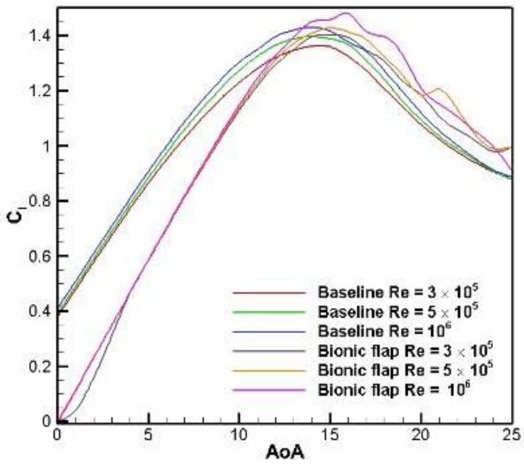

(a). Graph of C_l against changes AoA

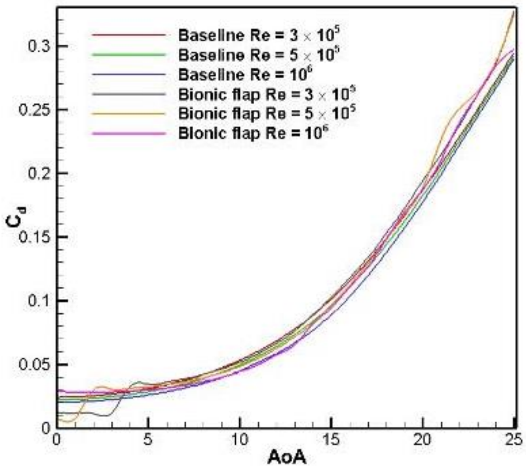

(a) Graph of C_d against changes AoA

Figure 6. Aerodynamic performance on airfoils with and without bionic flaps

Adding a bionic flap to the NACA 4415 airfoil causes a separation of the fluid flow to affect the drag and lift forces generated by the airfoil. As a result of the addition of the bionic flap, the pressure from the top of the airfoil is greater than the baseline. In contrast to the drag force, the addition of a bionic flap on the airfoil causes the drag force on the bionic airfoil to be bigger than the baseline airfoil. By reducing the lift force and increasing the drag force, the aerodynamic efficiency produced by the NACA 4415 airfoil with the bionic flap modification becomes smaller than the NACA 4415 baseline airfoil.

To describe the data on the increase in C_l and C_d from Figure 6, Table 2 is presented, which explains the percentage increase in data from C_d and C_l baseline NACA 4415 and modification with a bionic flap. At this stage, negative values symbolize a decrease, while positive values symbolize an increase. The value desired by C_l is an increase, while for C_d, it is expected to decrease. It can be seen that the increase in C_l data belonging to the three variations of the Reynolds number occurs from AoA = 14° to 25°. However, at Re = 3 × 10^5, the increase has occurred from AoA 13°. Then, at the percentage of C_d from Re = 10^6, there was an increase in AoA = 10°-13°. At the data percentage Re = 5 × 10^5, there is an increase in AoA = 0°-1°, and another growth occurs at AoA = 9°-14°. Then, at Re = 3 × 10^5, there is an increase in AoA = 0°-3° and AoA = 9°-13°.

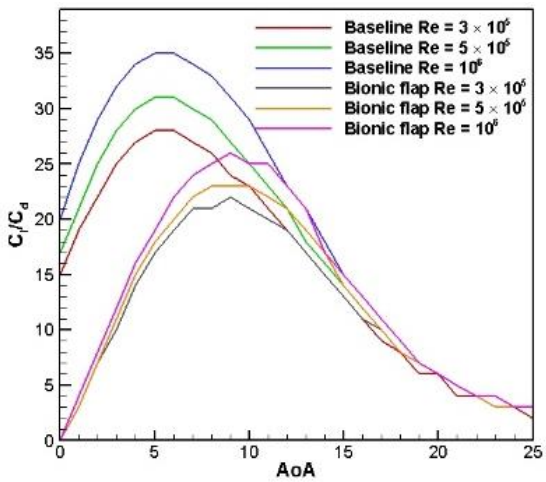

Figure 7. Graph of ratio C_l/C_d against AoA

As a complement to the data, a comparison of the C_l/C_d ratio data is presented, as shown in Figure 7. In this condition, the C_l/C_d ratio proves the effectiveness of adding a bionic flap to the airfoil. As shown in the figure, NACA 4415 baseline with Re = 10^6, the optimum C_l/C_d value is AoA = 6°. After adding the bionic flap, there is an increase in C_l/C_d, and the C_l/C_d value becomes optimum at AoA = 9°. The same thing happened to Re = 5 × 10^5 and Re = 3 × 10^5. With this increase in the C_l/C_d ratio, it can be said that the addition of a bionic flap to the airfoil can benefit airfoil maneuvers.

As a supporting argument in this study, the C_l-$C_{l\ baseline}$ data were compared with previous studies (Hao *et al.*, 2021). The results of the data comparison are shown in Figure 8. The Figure 8 shows that the C_l value at low AoA is below 0, which means that the C_l value has decreased. At high AoA, the C_l values of the four samples were above 0, which caused the airfoil to increase. Although this study uses a different type of airfoil than Hao's, adding a bionic flap has proven effective in increasing lift when the airfoil is at a high AoA.

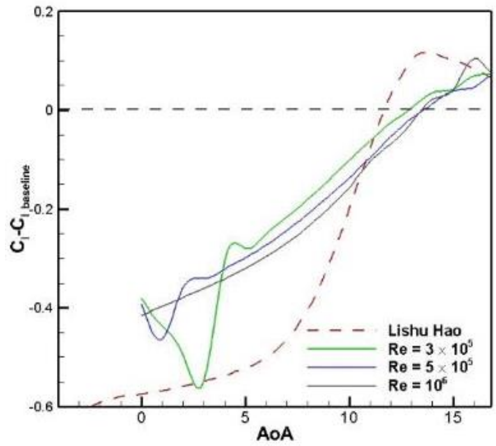

Figure 8. Graph of C_l-C_l baseline against AoA

To complete the data above, C_m data is presented, as shown in Figure 9. Two terms are often used in C_m: pitch up and down. Pitch-up is a condition where the C_m of an airfoil is positive. Besides that, in the pitch-up state, the airfoil generates a torque that rotates clockwise. The C_m value of an airfoil is only sometimes positive. In the pitch-down condition, C_m from the airfoil is negative, then the torque generated from the pitch-down state will rotate counterclockwise. In Figure 9, it can be seen that C_m from the six data is negative, so it can be concluded that there is a pitch-down condition. The airfoil's stability level is indicated by the value of C_m, which is close to zero. As can be seen in Figure 9, C_m produced by airfoils with bionic flaps tends to be more stable when compared to baseline airfoils at low AoA. In the bionic flap, the stability of the C_m value decreases with increasing AoA. Meanwhile, C_m from the baseline airfoil is stable at AoA = 15°-20°.

Table 2. Increase of C_l and C_d

AoA	Cl			Cd		
	Re = 10^6	Re = 5 × 10^5	Re = 3 × 10^5	Re = 10^6	Re = 5 × 10^5	Re = 3 × 10^5
0	-101.720%	-100.343%	-100.378%	45.199%	-64.805%	-50.728%
1	-78.008%	-94.226%	-91.426%	36.244%	-66.054%	-52.566%
2	-62.175%	-60.859%	-85.558%	33.379%	29.420%	-54.568%
3	-50.796%	-49.379%	-81.399%	26.909%	23.742%	-55.750%
4	-42.188%	-40.750%	-39.512%	20.847%	18.203%	15.778%
5	-35.342%	-33.810%	-32.417%	15.339%	13.106%	11.049%
6	-29.641%	-28.040%	-26.434%	10.148%	8.395%	6.688%
7	-24.726%	-22.995%	-21.062%	6.485%	4.582%	2.698%
8	-20.253%	-18.491%	-16.396%	3.252%	1.222%	0.192%
9	-16.033%	-14.447%	-12.164%	0.465%	-1.114%	-1.854%
10	-12.032%	-10.803%	-8.228%	-1.221%	-2.183%	-2.908%
11	-7.741%	-7.245%	-4.891%	-3.702%	-3.057%	-3.297%
12	-4.918%	-3.956%	-1.924%	-1.383%	-3.154%	-3.020%
13	-1.804%	-1.202%	0.293%	-2.188%	-2.615%	-2.194%
14	1.538%	0.889%	2.590%	6.475%	-1.812%	0.742%
15	2.949%	2.829%	3.133%	5.941%	0.696%	1.341%
16	7.607%	3.403%	5.264%	7.260%	1.348%	2.381%
17	5.453%	5.770%	5.856%	5.777%	2.275%	1.980%
18	9.709%	6.559%	8.324%	7.808%	2.489%	3.014%
19	11.136%	8.175%	7.935%	7.713%	3.221%	3.269%
20	7.983%	8.165%	10.004%	5.479%	3.307%	14.497%
21	9.066%	16.316%	8.170%	5.678%	11.569%	3.705%
22	10.391%	14.667%	8.190%	7.915%	11.217%	4.107%
23	10.276%	9.695%	8.522%	6.939%	6.726%	4.704%
24	9.310%	9.118%	8.150%	6.476%	6.600%	5.012%
25	2.571%	13.578%	13.185%	2.356%	11.253%	11.281%

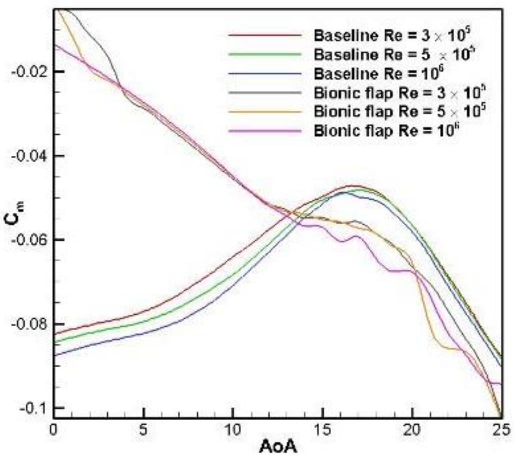

Figure 9. Graph of C_m against AoA

The difference in pressure distribution in the lower and upper sections is explained in the pressure contour visualization in Figure 10. The sample used in this visualization was drawn at AoA = 20°. It can be seen from the pressure contour visualization the pressure distribution in the upper section is much smaller than the pressure distribution in the lower area. This phenomenon then produces C_l so that the airfoil can be lifted. The addition of bionic flaps does not affect the lower part of the airfoil. However, on the upper, the addition of bionic flaps on the airfoil causes a decrease in pressure on the leading edge.

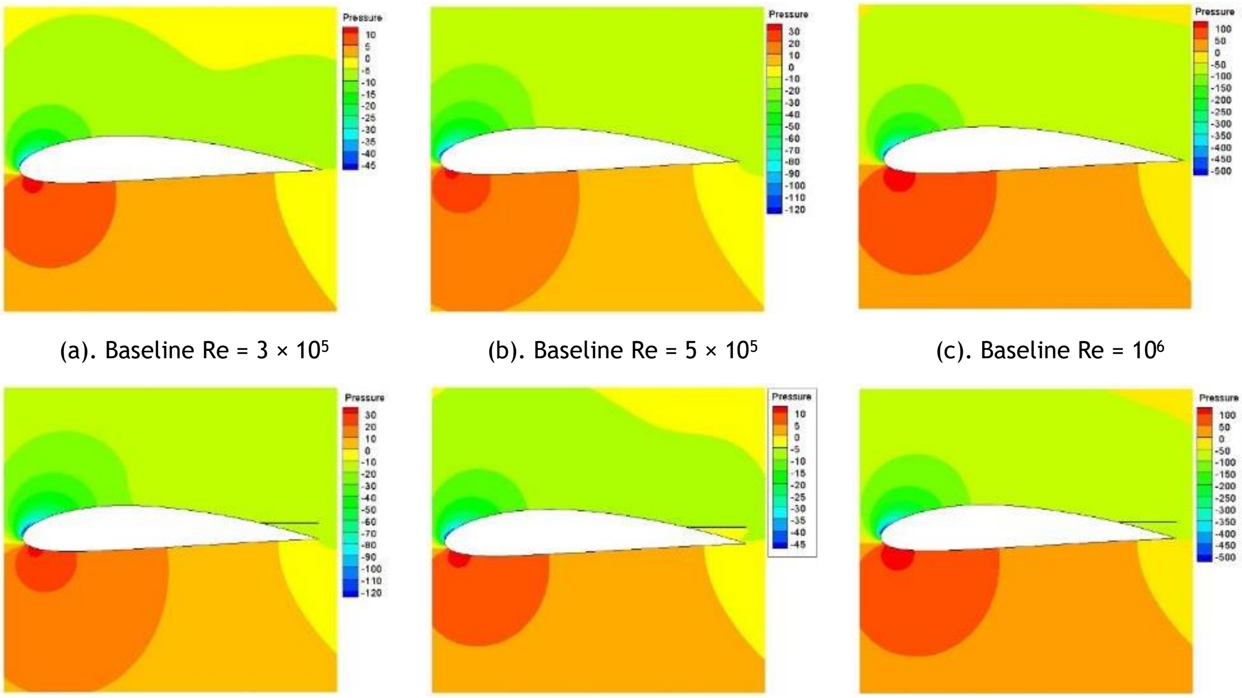

(a). Baseline Re = 3 × 10^5 (b). Baseline Re = 5 × 10^5 (c). Baseline Re = 10^6

(d). Bionic Re = 3 × 10^5 (e). Bionic Re = 5 × 10^5 (f). Bionic Re = 10^6

Figure 10. Pressure contour at 20°

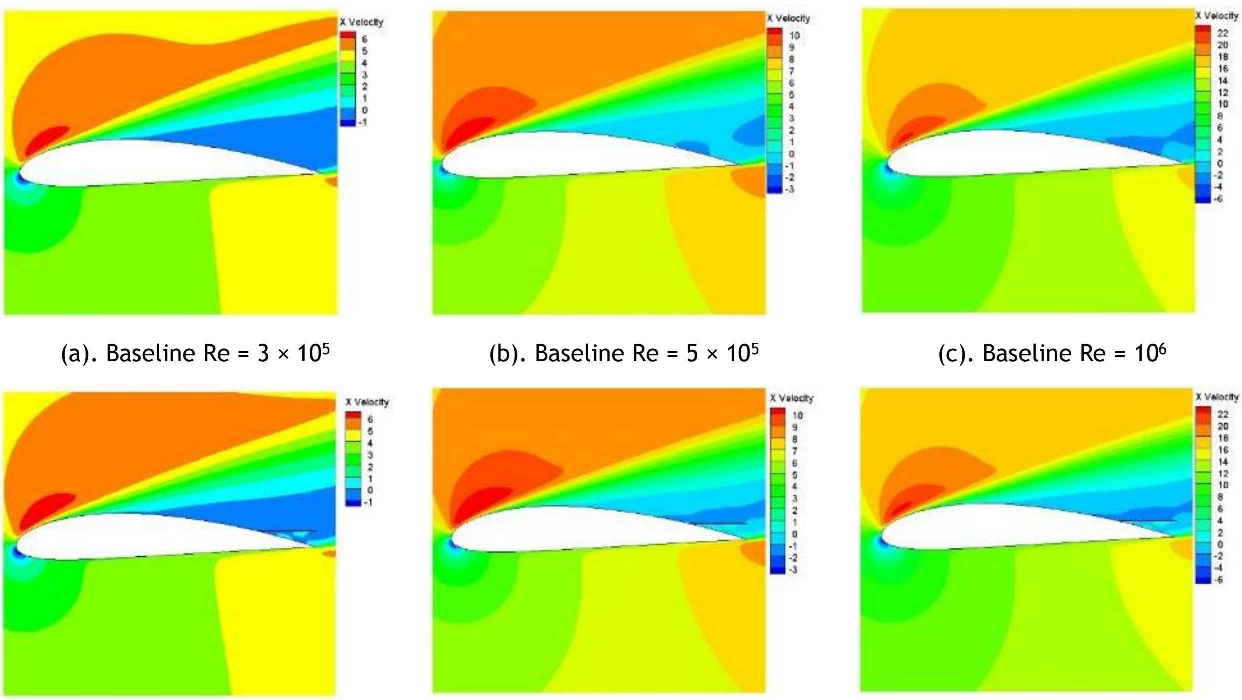

(a). Baseline Re = 3 × 10^5 (b). Baseline Re = 5 × 10^5 (c). Baseline Re = 10^6

(d). Bionic Re = 3 × 10^5 (e). Bionic Re = 5 × 10^5 (f). Bionic Re = 10^6

Figure 11. Velocity contour at 20°

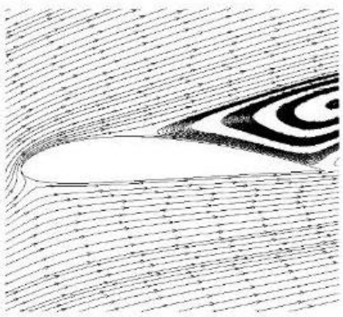
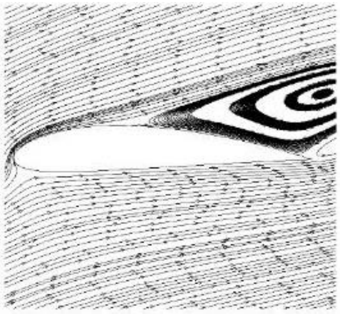
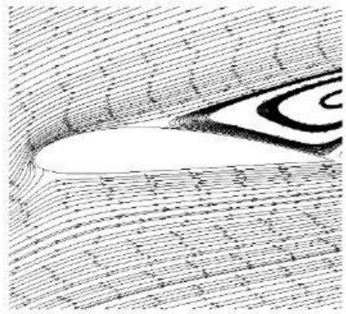

(a). Baseline Re = 3×10^5 (b). Baseline Re = 5×10^5 (c). Baseline Re = 10^6

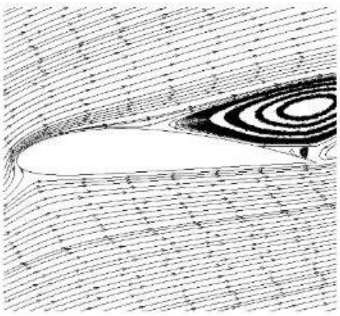
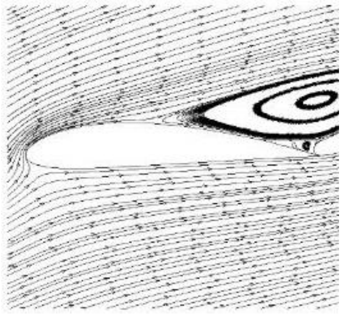
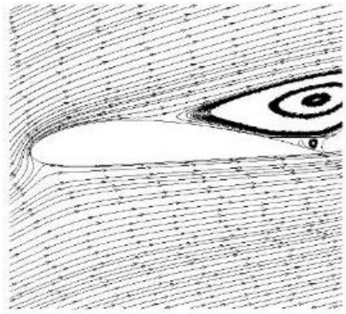

(d). Bionic Re = 3×10^5 (e). Bionic Re = 5×10^5 (f). Bionic Re = 10^6

Figure 12. Streamline velocity at 20°

Another contour used in this study is the velocity contour shown in Figure 11. Just like the pressure contour, a sample of the velocity contour was also taken at AoA = 20°. In Figure 11, it is explained that adding a flap does not affect the velocity in the lower part of the airfoil. However, the addition of bionic flaps on the upper leading edge causes an increase in airfoil velocity. Opposite the rear, there is a separation of the fluid flow, thereby reducing the rate on the airfoil's trailing edge.

Furthermore, we can see the velocity contour visualization from the streamlined velocity shown in Figure 12. From the depiction of the streamlined momentum, there is no impact of adding bionic flaps on the lower part. The upper part has a relatively large and severe flow separation at the trailing edge. However, there are two slight flow separations near the bionic flaps. The small flow separation in the bionic flap causes an increased pressure of the fluid flow separation at the trailing edge.

4. CONCLUSION

This paper was created to test the aerodynamic performance of the NACA 4415 airfoil. Computational tests were carried out on modifications with bionic flaps with variations of 3 Reynolds numbers Re = 106, Re = 5 × 105, dan Re = 3 × 105. The results of computational tests on these variations stated that adding bionic flaps to the airfoil causes the airfoil's Cl to decrease at low AoA. However, at high AoA, the bionic flap tends to give a higher Cl effect than the baseline. The increase in Cl occurs starting from AoA > 14°. In addition, the addition of bionic flaps can prevent stalls from occurring. On Cd, bionic flaps cause an increase in AoA from 10° to 13°. At high AoA, bionic flaps can reduce the pressure on the airfoil's leading edge and increase the velocity on the upper. So, it can be concluded that adding bionic flaps to the NACA 4415 airfoil can improve the aerodynamics of the airfoil at high AoA and prevent stalls.

REFERENCES

Aftab, S.M.A. *et al.* (2016) 'Turbulence Model Selection for Low Reynolds Number Flows', *PLOS ONE*, 11(4), pp. e0153755–e0153770.

Alom, N., Borah, B. and Saha, U.K. (2018) 'An insight into the drag and lift characteristics of modified Bach and Benesh profiles of Savonius rotor', *Energy Procedia*, 144, pp. 50–56.

Altman, A. and Allemand, G. (2016) 'Post-Stall Performance Improvement through Bio-inspired Passive Covert Feathers', in *54th AIAA Aerospace Sciences Meeting*. American Institute of Aeronautics and Astronautics.

Bardera-Mora, R. *et al.* (2019) 'Aerodynamic Flow Effects on Aircraft Carrier Takeoff Performance', *Journal of Aircraft*, 56(3), pp. 1005–1013.

Hao, L. *et al.* (2021) 'Numerical Simulation of Flow over Bionic Airfoil', *International Journal of Aerospace Engineering*, 2021, p. e5556463.

He, X. *et al.* (2019) 'Robust aerodynamic shape optimization—From a circle to an airfoil', *Aerospace Science and Technology*, 87, pp. 48–61.

Hoffmann, M.J., Reuss Ramsay, R. and Gregorek, G.M. (1996) *Effects of grit roughness and pitch oscillations on the NACA 4415 airfoil*. NREL/TP-442-7815. National Renewable Energy Lab. (NREL), Golden, CO (United States); The Ohio State Univ., Columbus, OH (United States).

Iskandar, W. and Julian, J. (2022) 'Study of Airfoil Characteristics on NACA 4415 with Reynolds Number Variations', *International Review On Modelling And Simulations (IREMOS)*, 15(3), pp. 162–171.

James, S.E. *et al.* (2018) 'Comparative study of boundary layer control around an ordinary airfoil and a high lift airfoil with secondary blowing', *Computers & Fluids*, 164, pp. 50–63.

Julian, J. *et al.* (2016) 'The Effect of Plasma Actuator Placement on Drag Coefficient Reduction of Ahmed Body as an Aerodynamic Model', *International Journal of Technology*, 7(2), pp. 306-313.

Julian, J. *et al.* (2022) 'Effect of Single Slat and Double Slat on Aerodynamic Performance of NACA 4415', *International Journal of Marine Engineering Innovation and Research*, 7(2), pp. 93-100.

Julian, J. *et al.* (2023) 'Aerodynamic Performance Improvement on NACA 4415 Airfoil by Using Cavity', *Jurnal Asiimetrik: Jurnal Ilmiah Rekayasa Dan Inovasi*, 5(1), pp. 135-142.

Karim, R.F. and Julian, J. (2018) 'Drag reduction due to recirculating bubble control using plasma actuator on a squareback model', in *ICET4SD 2017. The 2nd International Conference on Engineering and Technology for Sustainable Development*, Indonesia: MATEC Web of Conferences, p. 01108.

Kumar, P. and German, B.J. (2022) 'Optimization of High-Lift Systems at Takeoff Conditions Subject to Kinematic Constraints', *Journal of Aircraft*, 59(4), pp. 1098–1103.

Lang, X. *et al.* (2021) 'Aerodynamic performance of owl-like airfoil undergoing bio-inspired flapping kinematics', *Chinese Journal of Aeronautics*, 34(5), pp. 239-252.

Lew†, A.J., Buscaglia, G.C. and Carrica, P.M. (2001) 'A Note on the Numerical Treatment of the k-epsilon Turbulence Model*', *International Journal of Computational Fluid Dynamics*, 14(3), pp. 201–209.

Li, J., Bouhlel, M.A. and Martins, J.R.R.A. (2019) 'Data-Based Approach for Fast Airfoil Analysis and Optimization', *AIAA Journal*, 57(2), pp. 581–596.

Müller, L. *et al.* (2014) 'Aerodynamic Installation Effects of an Over-the-Wing Propeller on a High-Lift Configuration', *Journal of Aircraft*, 51(1), pp. 249–258.

Nair, N.J. and Goza, A. (2020) *Numerical study of a passively deployable flap for aerodynamic flow control*, p. X02.016.

Nair, N.J. and Goza, A. (2022) 'Fluid-structure interaction of a bio-inspired passively deployable flap for lift enhancement', *Physical Review Fluids*, 7(6), p. 064701.

Radespiel, R. and Heinze, W. (2014) 'SFB 880: fundamentals of high lift for future commercial aircraft', *CEAS Aeronautical Journal*, 5(3), pp. 239–251.

Raymer, D. (2018) *Aircraft Design: A Conceptual Approach, Sixth Edition*. 6th edn. American Institute of Aeronautics and Astronautics [Print].

Roache, P.J. (1994) 'Perspective: A Method for Uniform Reporting of Grid Refinement Studies', *Journal of Fluids Engineering*, 116(3), pp. 405–413.

Rubel, R.I. *et al.* (2016) 'Comparison of Aerodynamics Characteristics of NACA 0015 & NACA 4415'. Switzerland: Preprints MDPI.

Supriya, D. *et al.* (2019) 'Accurate higher order automated unstructured triangular meshes for airfoil designs in aerospace applications using parabolic arcs', *Aerospace Science and Technology*, 88, pp. 405–420.

Wu, L. *et al.* (2022) 'Using the combined flow control accessory to the aerodynamic performance enhancement of bio-inspired seagull airfoils', *Journal of Renewable and Sustainable Energy*, 14(2), p. 023302.

Xiao, H. *et al*. (2016) 'Quantifying and Reducing Model-Form Uncertainties in Reynolds-Averaged Navier-Stokes Simulations: A Data-Driven, Physics-Based Bayesian Approach', *Journal of Computational Physics*, 324, pp. 115–136.

Xie, Y.H. *et al*. (2016) 'Numerical investigation into energy extraction of flapping airfoil with Gurney flaps', *Energy*, 109, pp. 694–702.

Zhang, W. *et al*. (2015) 'Geometrical effects on the airfoil flow separation and transition', *Computers & Fluids*, 116, pp. 60–73.

Zhang, W. *et al*. (2017) 'Main characteristics of suction control of flow separation of an airfoil at low Reynolds numbers', *European Journal of Mechanics - B/Fluids*, 65, pp. 88–97.

Zhao, D.J. *et al*. (2015) 'Optimization of Suction Control on an Airfoil Using Multi-island Genetic Algorithm', *Procedia Engineering*, 99, pp. 696–702.

Zhao, Y. and Sushama, L. (2020) 'Aircraft Takeoff Performance in a Changing Climate for Canadian Airports', *Atmosphere*, 11(481), pp. 1–22.